EPJ Web of Conferences **29**, 00021 (2012)
DOI: 10.1051/epjconf/20122900021

Development of a new magnetocaloric material used in a magnetic refrigeration device

F. Guillou[1], U. Legait[2,3], A. Kedous-Lebouc[2] and V. Hardy[1,a]

[1]Laboratoire CRISMAT, UMR 6508, CNRS, ENSICAEN, 6 B[d] du M[al] Juin, F-14050 Caen 4, France
[2]Grenoble Electrical Engineering Laboratory- G2Elab, Grenoble INP – UJF Grenoble 1- CNRS UMR 5269, BP 46, F-38402 S[t]-Martin d'Hères, France
[3]Néel Institute, CNRS, UJF Grenoble INP, UPR 2940, BP 166, F- 38042 Grenoble 9, France

Abstract. Testing directly a magnetocaloric material in a magnetic refrigeration (MR) system is the best way to judge of its applicative potentialities. In this spirit, an oxide expected to show promising magnetocaloric properties around room temperature ($Pr_{0.65}Sr_{0.35}MnO_3$) was produced in large scale and shaped in order to build a regenerator. Magnetization, heat capacity, resistivity, thermal conductivity and a direct test in a MR device were carried out on this manganite. The results were compared to those observed in the reference material which is Gadolinium. The two main conclusions of these preliminary results are: (i) the $Pr_{0.65}Sr_{0.35}MnO_3$ actually displays not only a significant magnetocaloric effect but also a real refrigeration capability at room temperature; (ii) the temperature spans reached in these first experiments are even found to well compare with those obtained with Gd.

1 Introduction

While the needs in the fields of refrigeration and air conditioning have known an incredible growth in recent decades, the current environmental requirements restrict more and more traditional technologies. One of the alternatives to the conventional technology (vapor compression/expansion) is the magnetic refrigeration (MR), based on the use of magnetocaloric effect (MCE) materials. This emerging technique is indeed characterized by a higher energy efficiency as well as the absence of global-warming gases as still used nowadays in conventional refrigerators.

At the present time, most of the RM prototypes are based on gadolinium, a material exhibiting a large MCE at room temperature (RT), even though it is quite expensive and subject to technical problems such as corrosion in aqueous environment. In the last ten years, most of the researches have been focused on the investigation of some families of intermetallic compounds showing the so-called giant MCE [1]. However, problems remain for the implementation of these materials in MR systems. Beside basic questions dealing the first-order nature of these transitions, the use of these materials also faces a series of practical concerns, related to cost, difficulty of synthesis, and ageing in operational conditions (corrosion, crumbling, etc).

It turns out that it is precisely on these issues that oxides can claim some advantages, which could compensate for their lower performance in terms of intrinsic MCE. On more general grounds, it must

[a] e-mail : vincent.hardy@ensicaen.fr

be emphasized that although the MCE is at the heart of a RM device, many other physical properties are involved in such a complex magneto-thermal apparatus. Thereby, only direct tests in a RM demonstrator are really reliable to judge of the potentiality of any material. Since more than ten years, demonstrators and more industrially-oriented prototypes are developed in the laboratory G2Elab [2, 3].

In this context, the aim of the present study was to investigate the performances of an oxide, compared to the "benchmark" material that is gadolinium. This experiment was carried out in a demonstrator specially designed to test various materials: it operates around room temperature, involves a moderate magnetic field of 0.8 T and uses water as exchange fluid.

The first step was to identify an oxide complying with a series of criteria, dictated by the operational conditions of the prototype and by the common constraints to any commercial applications:

- MCE reflecting the largest expectable value for an oxide in the operating conditions: room temperature (i.e. centered in the range 291 K-295 K) and moderate magnetic field (B_{max} = 0.8 T)
- No toxic or too expensive elements
- Limited number of elements to facilitate the control of reproducibility
- Synthesis procedure compatible with a large-scale production (typically half a kilogram).
- Ability to be shaped in the form of thin plates
- Corrosion resistant material

The best oxides for MCE around RT are manganese perovskites $R_{1-x}AE_xMnO_3$ with a ratio $Mn^{3+}/ Mn^{4+} \approx 2$, which allows to combine large magnetizations and high T_C. The most studied compounds were the $La_{1-x}(Ca, Sr)_xMnO_3$ with $x \approx 1/3$. This series is generally regarded as the archetypical example of magnetocaloric oxides at RT [4, 5]. However, there are other systems leading to similar performances that can also be considered. It is the case for instance of the series $Pr_{1-x}Sr_xMnO_3$ [6], which has the advantage to contain fewer elements, so to have an easier synthesis and a better control of T_C. This system has been relatively understudied in terms of MCE: up to now, only few results have been reported for x = 0.37 and x = 0.4, but at temperatures above 300 K [7, 8], while for x = 0.45, a T_C at room temperature was recently observed, but associated with a modest MCE [9].

Following the phase diagram of [6], we decided to investigate in detail the substituting range ($0.34<x<0.37$) in order to adjust T_C within the required interval, while generating large magnetizations. Then, characterizations of the basic magnetocaloric properties, i.e. the isothermal entropy change $\Delta S(T)$ and the adiabatic temperature change ΔT_{ad} (T), were derived from standard indirect methods. Additional physical properties involved in RM devices were also investigated. Finally, this oxide was inserted into our demonstrator to evaluate its refrigerating capability. These preliminary results are discussed in comparison to those observed with Gd in similar conditions.

2 Experimental details

2.1 RM apparatus

Our MR device operates on the principle of the AMRR (Active Magnetic Regenerative Refrigeration) cycle. Its global design is based on a reciprocating geometry (vertical) where the moving part is the magnet. This magnet is made of $Nd_2Fe_{14}B$ pieces arranged in a Halbach geometry leading to about 0.8 T in the center of it. A Plexiglas tube contains the regenerator and two pistons which ensure the movement the heat transfer fluid (water). (see review [10] for photos).

The regenerator is 50 mm long in the direction of flow, and roughly has square cross section ($\approx 20*20$ mm^2). It consists of a stack of thin plates (typically 1 mm thick), with spacers to control the distance between them (typically 0.3 mm). This device does not include real heat exchangers at each end of the fluid reservoir, in such a way that only the performance in terms of temperature span (i.e. difference between the temperature of the hot and cold sides of the regenerator) can be studied.

2.2 Material production

The $Pr_{0.65}Sr_{0.35}MnO_3$ material was prepared by using standard solid state reaction. Stoeichiometric quantities of Pr_6O_{11}, $SrCO_3$ and MnO_2 were mixed and calcined at 1200 °C for 24 hrs in air. Then the resulting powder (≈ 0.6 kg) was regrinded and pressed in form of blocks with sides of 40 mm. An organic binder was added to ensure the cohesion of the blocks. Its removal is performed during the final sintering at 1500 °C during 48 hrs in air. X-ray diffraction data demonstrated the purity of the samples and led to values of cell parameters in line with the literature.

In order to obtain plates with the desired dimensions (20*25*1 mm^3), these blocks were cut with a laboratory circular saw and the plates were then butted two by two in order to get the 50 mm length of the regenerator. Figure 1 illustrates the whole process from the sintered block up to the final regenerator.

Since several batches (blocks) were needed to manufacture the regenerator, great attention had to be paid to the reproducibility of the preparation procedure.

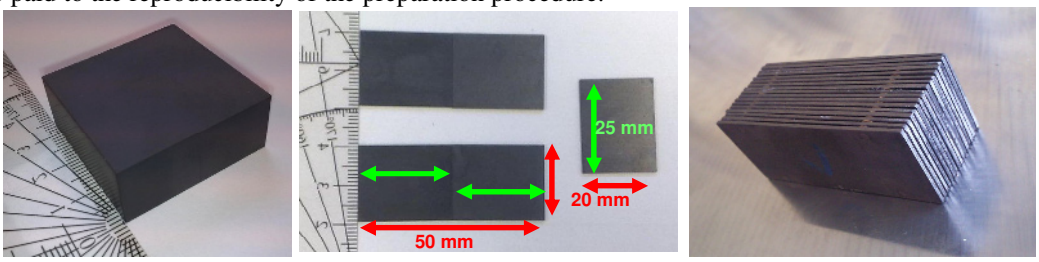

Fig. 1. From left to right: a block of $Pr_{0.35}Sr_{0.35}MnO_3$; some $Pr_{0.35}Sr_{0.35}MnO_3$ slabs with their dimensions after cutting; configuration of the regenerator made of a stack of parallel slabs (the 17 slabs of Gd)

2.3 Physical measurements

Magnetization, heat capacity, resistivity and thermal conductivity were measured by means of a commercial device (Physical Properties Measurements system, Quantum Design). Isothermal $M_T(B)$ curves were recorded after a zero-field cooling from 310 K, while isofield $M_B(T)$ were recorded using a zero-field-cooled-warming procedure. The heat capacity curves were registered upon warming in 0 and 1T, using a 2τ analysis method. Resistivity measurements in zero-field were performed by the standard four-probes technique, at temperatures from 5 to 325 K. The thermal conductivity was measured from 150 to 325K, in zero-field, by a four point steady-state method using a homemade sample holder.

3 Results and discussion

3.1 Basic properties

Since the T_C in $Pr_{1-x}Sr_xMnO_3$ was found to be very sensitive to the substitution level (displacement of about 4 K per % of Sr, in this range of x), several x values had to be investigated. On the $M_B(T)$ curve measured in B=0.05 T shown Figure 2A, one can observe that the T_C of $Pr_{0.65}Sr_{0.35}MnO_3$ (295 K), is within the acceptable temperature range for the test. This value of T_C is confirmed by the specific heat curve (Figure 2B) which exhibits a clear transition around 294 K. Note the lambda shape of this anomaly, which is typical of a second-order magnetic transformation. As expected, one can also observe on both the magnetic and heat capacity data that the field application makes the transition to be considerably broadened while being slightly shifted towards higher temperatures.

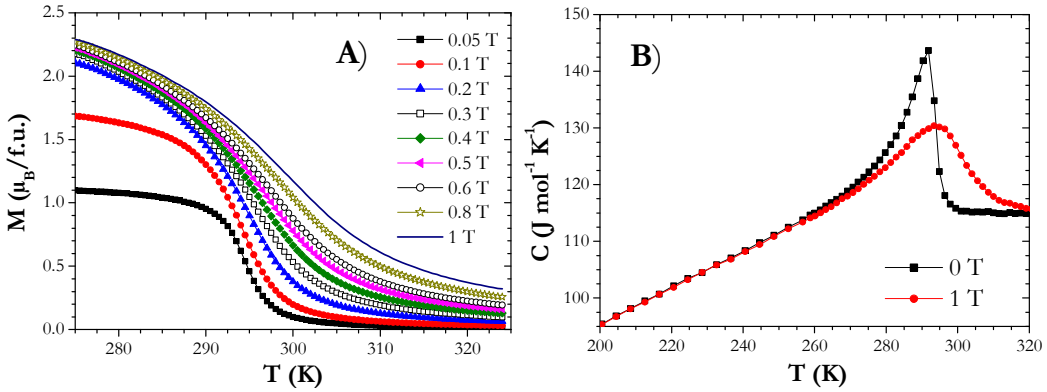

Fig. 2. (A) $M_B(T)$ curves recorded in various magnetic fields. (B) Temperature dependence of C in zero-field and in B=1T.

The MCE can be quantified as an entropy variation induced by a field variation at a given temperature, ΔS (T, ΔB). In order to derive these values, the common method based on the Maxwell equation [1]

$$\Delta S(T,\Delta B) = \frac{\partial}{\partial T}\int_0^B M(T,B')dB' \tag{1}$$

can be applied to series of isothermal magnetizations curves $M_T(B)$ or isofield curves $M_B(T)$. In our case, both types of data were used.

The second method to derive ΔS values is based on calorimetric data. If one measures the heat capacity in zero field and in the magnetic field B, the entropy curves can be determined by the relationship [1]:

$$S(T,B) = \int_0^T \frac{C(T',B)}{T'}dT' \cdot \tag{2}$$

Then, a simple subtraction is expected to yield the isothermal entropy change:

$$\Delta S(T,\Delta B) = S(T,B) - S(T,0) \cdot \tag{3}$$

With this calorimetric method, one can also obtain the second quantity of the MCE, i.e. the adiabatic temperature change $\Delta T_{ad}(T, \Delta B)$. These values were derived from the entropy curves using the equation:

$$\Delta T_{ad}(T,\Delta B) = \left[T_B(S) - T_0(S)\right]_{S_0(T)} \tag{4}$$

Figure 3 shows the ΔS(T) curve for a field change of ΔB=1T , that were derived from our three sets of data. First of all, one observes a remarkable agreement between these three approaches about the intensity of the peak [ΔS (T, ΔB= 1T) ≈ -2.3 $Jkg^{-1}K^{-1}$], while its location lies within a very restricted temperature interval [294-295 K].

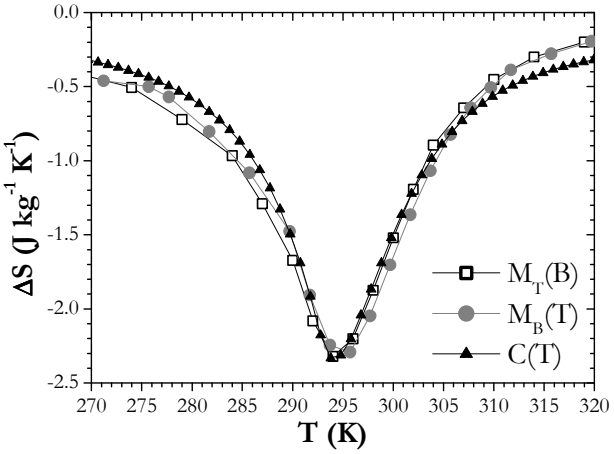

Fig. 3. ΔS(T) curves resulting from the analysis of magnetization and heat capacity data for a field change of ΔB=1T.

The $\Delta T_{ad}(T)$ curve in case of a field change ΔB=1T is shown on Figure 4. Consistently with the ΔS(T) curve, the peak is found to be located just below 295 K. One can also note it is the temperature corresponding to the crossing between the C(T) curves in zero-field and in B=1T (Figure 2B).

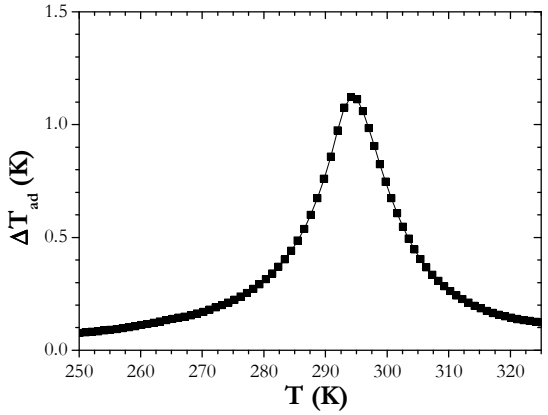

Fig. 4. Temperature dependence of the adiabatic temperature change in $Pr_{0.65}Sr_{0.35}MnO_3$, measured for a field change of 1T.

Two other physical properties that may play a role in magnetic refrigeration were recorded. The resistivity curve (Figure 5A) displays a large drop below T_C, which results from the appearance of ferromagnetism associated to the double exchange mechanism. The evolution of the thermal conductivity vs. T is shown on Figure 5B. Superimposed onto a global increase as the temperature is increased, one clearly notices the presence of a small dip at T_C, which is another expected hallmark associated with the onset of ferromagnetism in these manganites.

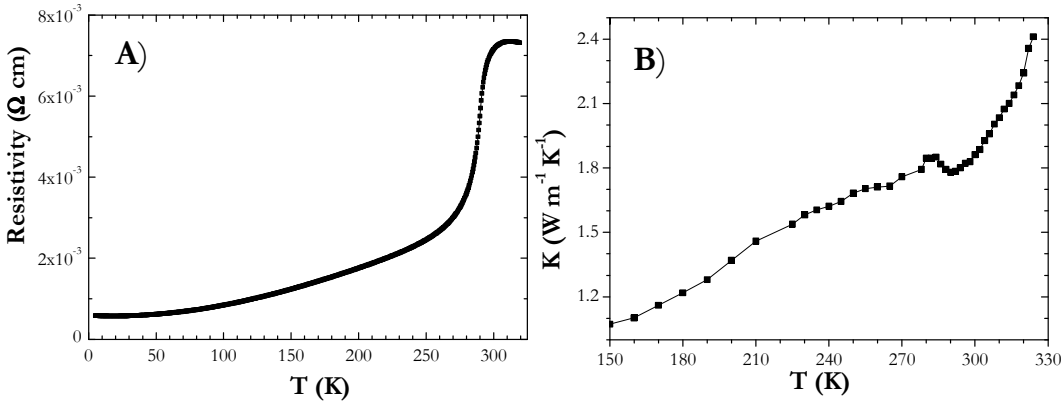

Fig. 5. Temperature dependence of electrical resistivity (A) and thermal conductivity (B), in zero-field.

To sum up, Table 1 gathers the main physical parameters of $Pr_{0.65}Sr_{0.35}MnO_3$ that are expected to be involved in a MR device. The correspondent values are given for the « reference » material that is Gd.

Table 1. Properties of $Pr_{0.65}Sr_{0.35}MnO_3$ and Gd. The values given for κ, C and resistivity are for $T=T_C$ and B=0.

Compound	T_C (K)	$\lvert \Delta S_{max} \rvert$ ΔB=1T ($Jkg^{-1}K^{-1}$)	ΔT_{ad}-max ΔB=1T (K)	ΔT_{ad} max ΔB=0.8T (K)	K at T_C $Wm^{-1}K^{-1}$	C at T_C $Jkg^{-1}K^{-1}$	Resistivity at T_C Ωm	relative density	Ref.
$Pr_{0.65}Sr_{0.35}MnO_3$	295	2.3 (0)	1.1	0.9	1.8	580	$7.5\ 10^{-5}$	≈5.8	Present work
Gd	294	2.3	2.0	1.6	10.6	230	$\approx 1.3\ 10^{-6}$	≈7.9	[11]

3.2 Comments regarding applications in MR

Firstly, one can note that the maximum of ΔS (= -2.3 $Jkg^{-1}K^{-1}$, ΔB=1T) is well consistent with the values reported in the literature for the closest compositions [7, 8]. More importantly, this maximum of ΔS is actually comparable to the best values reported in manganites around room temperature [5]. The same is true when considering ΔT_{ad}, even though there are much less data in the literature about this parameter.

Compared to Gd, $Pr_{0.65}Sr_{0.35}MnO_3$ has a similar ΔS_{max}, but it is clear that its ΔT_{ad} is significantly lower. It turns out that this feature directly reflects the larger value of heat capacity in the manganite. On the other hand, it deserves to be noted some authors claimed that a large heat capacity might be beneficial in terms of cooling capacity (at constant ΔT_{ad}) [12]. As for the thermal conductivity (κ), the situation is less prone to controversy, since it is quite obvious that decreasing κ limits the heat transfer and therefore the performance of a regenerator. This fact is a weak point for $Pr_{0.65}Sr_{0.35}MnO_3$ whose thermal conductivity is about 6 times lower than that of Gd. In other respects, we note that the large electrical resistivity found in $Pr_{0.65}Sr_{0.35}MnO_3$ is rather a positive point. Indeed, upon field cycling, a source of losses for the MR devices comes from the eddy current heating. Having a resistivity more than 50 times higher than in Gd, this problem should be drastically reduced in $Pr_{0.65}Sr_{0.35}MnO_3$.

From a practical viewpoint, it must be kept in mind that the slabs constituting the regenerator in $Pr_{0.65}Sr_{0.35}MnO_3$ come from different blocks. In order to check the homogeneity of these pieces, a few ΔS data points were evaluated for each block, by using the magnetic method based on $M_T(B)$ curves. Figure 6A shows the ΔS values measured in the 5 blocks. A very satisfying overall agreement is observed.

In the introduction, we also mentioned that one important issue in favour of the oxides was their expected resistance to corrosion. Figure 6B displays the $\Delta S(T)$ curves of a $Pr_{0.65}Sr_{0.35}MnO_3$ sample stored in water and periodically measured. After one year and six months, one observes that the MCE of this manganite is still unmodified, which evidences its resistance to this source of "ageing".

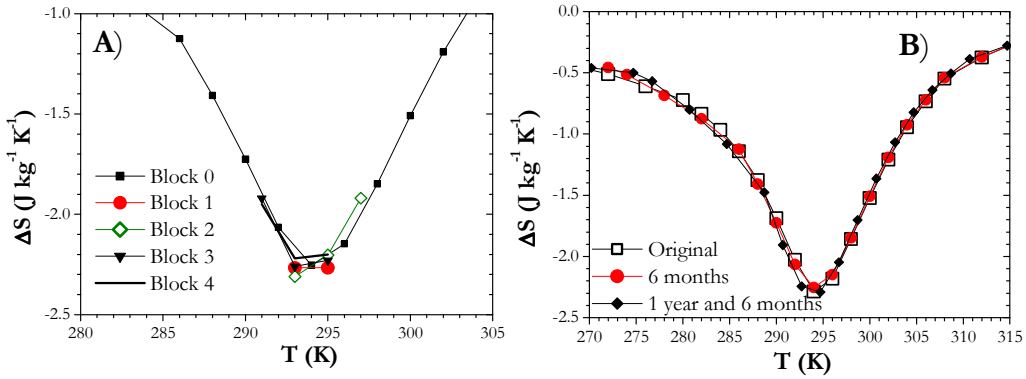

Fig. 6. (A) Control of reproducibility between different batches in terms of $\Delta S(T, \Delta B=1T)$ on the basis of magnetization $M_T(B)$ measurements. (B) Influence of the storage time in water on the $\Delta S(T, \Delta B=1T)$ curve.

3.3 Direct tests of MR with $Pr_{0.65}Sr_{0.35}MnO_3$. Comparison with Gd

The regenerator with the oxide was prepared to resemble a previous one made with Gd. We used the same slab thickness (1 mm) and the same inter-spacing (0.3 mm). For some practical reasons, however, we had to include only 11 slabs in the "oxide" regenerator, whereas they are 17 in the "Gd" regenerator.

For these preliminary results, only two sets of parameters were investigated in both regenerators. Starting from an initial temperature in the range 20.6-21.0°C and using a frequency of 0.18 Hz, two values of the flow rates (0.5 and 1 mL/s) were studied in each regenerator.

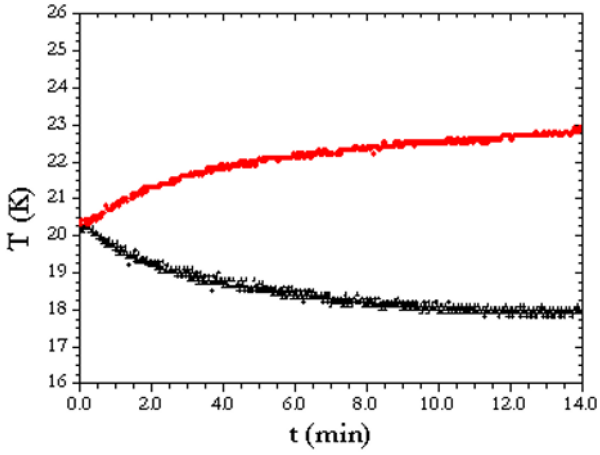

Fig. 7. Time dependence of Hot sink (circles) and cold sink (crosses) temperatures of the AMRR test device equipped with the $Pr_{0.65}Sr_{0.35}MnO_3$ regenerator (f=0.18 Hz, fluid flow rate=0.5 mLs^{-1}).

Figure 7 shows the evolution versus time of the temperatures at the "cold side" and at the "hot side" of the oxide regenerator. One can clearly observe the achievement of a substantial ΔT_{span} after about 10 min (i.e. about 100 cycles). Without any specific adjustment on this configuration initially used for Gd, the manganite directly provides us with a large ΔT_{span}, reaching about 5.0 K. This performance is close to those recently obtained in 2011 with a manganite of the series $La_{1-x}(Ca,Sr)_xMnO_3$, which was the first report of magnetic refrigeration based on an oxide [13, 14].
The results obtained on the "$Pr_{0.65}Sr_{0.35}MnO_3$" and "Gd" regenerators, for the two sets of parameters, are reported in Table 2.

Table 2. Results and parameters of RM tests for Gd and $Pr_{0.65}Sr_{0.35}MnO_3$ regenerators (see text).

	Gd	**$Pr_{0.65}Sr_{0.35}MnO_3$**
$\dot{V}_f$ **= 0.5 mL/s** f = 0.18 Hz	**ΔT_{span} = 6.3 K** **ζ = 3.9** **(NTU=146, U= 0.17)**	**ΔT_{span} = 5.0 K** **ζ = 5.6** **(NTU=96, U= 0.14)**
$\dot{V}_f$ **= 1 mL/s** f = 0.18 Hz	**ΔT_{span} = 9.8 K** **ζ = 6.1** **(NTU=73, U= 0.33)**	**ΔT_{span} = 4.0 K** **ζ = 4.5** **(NTU=48, U= 0.28)**

When comparing the two regenerators, one observes that the ΔT_{span} for $Pr_{0.65}Sr_{0.35}MnO_3$ are systematically lower than for Gd, even though they remain of the same order of magnitude. Although the difference in the number of slabs may play a role, this behavior most likely reflects the substantial difference existing between the ΔT_{ad} of these two materials (see Table 1). Accordingly, when comparing the two regenerators, it is interesting to consider also the ratio $\zeta = \Delta T_{span} / \Delta T_{ad}$, which is the amplification factor induced by the AMRR process itself. One observes that this factor takes very similar values for both regenerators. One can even note that it is larger with $Pr_{0.65}Sr_{0.35}MnO_3$ than with Gd, for the lowest flow rate.

When considering the results of Table 2, a striking difference between the two materials is about the influence of the flow rate: both ΔT_{span} and ζ increase with the flow rate for Gd, whereas the opposite is observed with $Pr_{0.65}Sr_{0.35}MnO_3$. Generally, when comparing different regenerators or working conditions in the same RM device, two dimensionless parameters are used: the Number of Transfer Units (NTU) and the Utilization (U) [15].
The NTU is related to the heat exchange between the solid and the fluid. It is defined by the relationship:

$$NTU = \frac{hA}{\dot{m}_f C_f} \tag{5}$$

where h is the heat transfer coefficient, A the total exchange surface, $\dot{m}_f$ the mass flow rate of the fluid and C_f the specific heat of the fluid. On the basis of theoretical estimates and numerical simulations, we assume h ≈ 9000 Wm^{-2} K^{-1}. Considering the geometry of the slabs (length=50 mm and width=20 mm), one can thus calculate the NTU for the two regenerators and at each flow rate. The results are reported in table 2.

The utilization factor, U, is the heat capacity ratio of the fluid to the solid, when considering for the former the mass of fluid *that is displaced along each blow* ($m_{f\text{-}disp.}$). This leads to the formula:

$$U = \frac{m_{f-disp.}\ C_f}{m_s\ C_s} \tag{6}$$

where C_s and C_f are the specific heats of the solid and the fluid, respectively, while m_s is the mass of solid and $m_{f-disp} = \dot{m}_f / 2f$ (f is the frequency). Introducing the volume flow rate ($\dot{V}_f = \dot{m}_f / \rho_f$), as well as the density (d_s) and volume (V_s) of the solid, one can write:

$$U = \frac{\dot{V}_f\ C_f}{2\,d_s\ V_s\ C_s\ f} \tag{7}$$

Assuming for Gd a density d_{Gd}=7.9 and a volume V_{Gd} = 17 cm^3 (note that in the present case each slab is about 50×20×1 mm^3=1 cm^3), one can calculate the U values for the two flow rates (see Table2).

It is commonly considered that there is an optimal value of U maximizing the cooling capacity [16] and the higher is the NTU, the better this maximum would be [15]. Although not connected to heat exchangers, our device is subjected to some thermal load owing to sizeable heat losses to the environment, in such a way that ΔT_{span} exhibits an optimum as a function of U. In our demonstrator, this optimum was found to be around U= 0.5 with Gd, a feature which is consistent the evolution of ΔT_{span} observed in Table 2 for Gd.

In the case of $Pr_{0.65}Sr_{0.35}MnO_3$, a possible reason for lower performances could be the smaller NTU, but this does not explain the opposite trend that is observed in the evolution of ζ versus U. Actually, it should be kept in mind that one of the main differences between Gd and $Pr_{0.65}Sr_{0.35}MnO_3$ is about the thermal conductivity κ. This physical property does not explicitly appear in the usual expressions of U and NTU, which indeed assume a perfect heat transfer between the solid and the fluid. In the case of $Pr_{0.65}Sr_{0.35}MnO_3$, which has a κ about 6 times lower than in Gd, it turns out that this assumption is probably no longer valid. Indeed, one estimates that the Biot number with the oxide (Bi ≈ 2.5) reaches a value too high to still assume the "thin plate picture" from the thermal viewpoint. Qualitatively, such a temperature gradient across the thickness of the plates would lead them to have an inactive core. As a consequence, the thermally active mass ($m_{s\text{-}eff}$) to be considered is significantly less than the total mass of regenerator (m_s), a fact that could induce a shift between the calculated U values and the effective ones. This phenomenon would be much more prominent in manganites than in Gd (Bi ≈ 0.4).

Obviously, more work is needed to address this issue, in particular more experimental points to draw a maximum on a ΔT_{span}(U) curve. Moreover, improvement of the modelization to explicitely take into account this κ parameter in the analysis of regenerators would be highly welcome. Lastly, we note that a practical way to counterbalance a smaller κ would consist in reducing the thickness of the plates (to recover a situation where $m_{s\text{-}eff} \approx m_s$). These works are currently in progress.

4 Conclusion

In the present work, the selection, production, characterization, and a direct test in MR device at room temperature were presented for an oxide. The maximum temperature span obtained with the $Pr_{0.65}Sr_{0.35}MnO_3$ regenerator in the AMRR device was 5.0 K without any optimization, suggesting the possibility for large future performances. We also note that the opportunity of adjusting the T_C of $Pr_{1-x}Sr_xMnO_3$ could be a promising way to produce a multi-component regenerator with T_C distributed along it.

Acknowledgments

The authors thank S. Marinel and J. Lecourt (CRISMAT – CNRT, Caen) for their help, and acknowledge the financial support of the "Programme Interdisciplinaire ENERGIE" of CNRS and the ANR "Magcool" (France) for this project.

References

1. K. A. Gschneidner Jr., V. K. Pecharsky and A. O. Tsokol, Rep. Prog. Phys. **68**, 1479 (2005)
2. C. Dupuis, A. J. Vialle, U. Legait, A. Kedous-Lebouc, D. Ronchetto, New investigations in magnetic refrigeration device, AMR cycle and refrigerant bed performance evaluation, *Third International Conference on Magnetic Refrigeration at Room Temperature*, IIF-IIR, 437 (2009)
3. U. Legait, A. Kedous-Lebouc, New investigations in a FLUENT 2D Numerical tool for active magnetic regenerator modelling, *Fourth International Conference on Magnetic Refrigeration at Room Temperature,* IIF-IIR (2010)
4. A. R. Dinesen, S. Linderoth and S. Mørup, J. Phys.: Condens. Matter. **17**, 6257 (2005)
5. M.-H. Phan, S.-C. Yu, J. Magn. Magn. Mater. **308**, 325 (2007)
6. C. Martin, A. Maignan, M. Hervieu, and B. Raveau, Phys. Rev. B **60**, 12191 (1999)
7. M.-H. Phan and H.-X. Peng, S.-C. Yu, J. Appl. Phys. **97**, 10M306 (2005)
8. S. Zemni, M. Baazaoui, J. Dhahri, H. Vincent, M. Oumezzine, Mat. Lett. **63**, 489 (2009)
9. J. Fan, L. Pi, L. Zhang, W. Tong, L. Ling, B. Hong, Y. Shi, W. Zhang, D. Lu, Y. Zhang, Physica. B **406**, 2289 (2011)
10. B. Yu, M. Liu, P. W. Egolf, A. Kitanovski, Int. J. Refrig. **33**, 1029 (2010)
11. A. Lebouc, F. Allab, J.-M. Fournier and J.-P. Yonnet, Tecniques de l'ingénieur. **RE-28**, 1 (2005)
12. K. Engelbrecht and C. R. H. Bahl, J. Appl. Phys. **108**, 123918 (2010)
13. N. Pryds, F. Clemenc, M. Menon, P. H. Nielsen, K. Brodersen, R. Bjørk, C. R. H. Bahl, K. Engelbrecht, K. K. Nielsen, A. Smith, J. American Ceramic Soc., in press (2011)
14. K. Engelbrecht, C. R. H. Bahl, K. K. Nielsen, Int. J. Refrig. **34**, 1132 (2011)
15. P. Li, M. Gong, G. Yao, J. Wu, Int. J. Refrig. **29**, 1259 (2006)
16. G. Tagliafico, F. Scarpa, F. Canepa, Int. J. Refrig. **33**, 286 (2010)